

Orbital-angular-momentum mixing in type-II second-harmonic generation

Leonardo J. Pereira, Wagner T. Bueno, Daniel S. Tasca, Kaled Dechoum, and Antonio Z. Khoury*

Instituto de Física, Universidade Federal Fluminense, Avenida General Milton Tavares de Souza S/N, 24210-340 Niterói RJ, Brazil

(Received 19 July 2017; published 27 November 2017)

We investigate the nonlinear mixing of orbital angular momentum in type-II second-harmonic generation with arbitrary topological charges imprinted on two orthogonally polarized beams. Starting from the basic nonlinear equations for the interacting fields, we derive the selection rules determining the set of paraxial modes taking part in the interaction. Conservation of orbital angular momentum naturally appears as the topological charge selection rule. However, a less intuitive rule applies to the radial orders when modes carrying opposite helicities are combined in the nonlinear crystal, an intriguing feature confirmed by experimental measurements.

DOI: [10.1103/PhysRevA.96.053856](https://doi.org/10.1103/PhysRevA.96.053856)

I. INTRODUCTION

The ability to control different degrees of freedom of a light beam is essential for both quantum and classical communication protocols. In this context, orbital angular momentum (OAM) has proved to be a potentially useful tool and has motivated a fair amount of research work with potential applications to quantum and classical information processing [1]. In the quantum domain, qubits and qudits can be encoded on either Laguerre-Gaussian (LG) or Hermite-Gaussian (HG) modes, which combined with the photon polarization allows creation of entanglement between internal photonic degrees of freedom. Many works have been devoted to schemes for implementing and applying this spin-orbit coupling [2,4–12]. Beyond the intrinsic beauty of this subject, one may find interesting applications to quantum information tasks like optical communication [13,14], teleportation schemes [15–21], alignment-free quantum cryptography [22–24], controlled gates for quantum computation [25,26], quantum simulations [27,28], and metrology [29–31]. Quite curiously, the presence of spin-orbit structures in an optical beam can be characterized by inequality criteria similar to those used to witness entanglement in quantum mechanics [32–39]. The interplay between spin and spatial degrees of freedom also plays an important role in the noise properties of vertical-cavity surface-emitting lasers [40].

Orbital-angular-momentum exchange in nonlinear interactions has been extensively studied and is still a fruitful domain. It has already been investigated in frequency up [41–49] and down [50–52] conversion, optical parametric oscillation [53–56], four-wave mixing in atomic vapors [57–59], and high harmonic generation [60,61]. A detailed theoretical treatment of the orbital-angular-momentum transfer in different nonlinear processes can also be found in Ref. [62].

The control of the nonlinear optical interaction through polarization has been also considered both in the quantum [3,4] and classical regimes [44,63]. In these examples, the phase-match condition imposes simple arithmetic relations among the topological charges of the interacting modes [44,46]. In the seminal works on second-harmonic generation with OAM beams, the intuitive charge doubling condition was demonstrated and remained as a natural assumption until other

degrees of freedom were brought into play. In type-II second-harmonic generation with LG modes, we have demonstrated different topological charge operations controlled by the polarizations of the interacting beams. Actually, these operations are a natural consequence of selection rules arising from the spatial overlap among the interacting modes. In cylindrical coordinates, the angular part of the spatial overlap trivially leads to topological charge conservation. The nonlinear wave mixing may also cause the appearance of radial structures [47,64–67].

In this paper we perform a detailed study about orbital-angular-momentum mixing in collinear type-II second-harmonic generation. Multimode coupling is considered in connection with OAM addition and the selection rules are derived based on the spatial overlap between the modes participating in the nonlinear process. One curious consequence of these selection rules is the appearance of higher radial orders when opposite topological charges are added. This intriguing feature of the nonlinear interaction is theoretically derived and experimentally confirmed. We also derive the analytical solution for the nonlinear dynamical equations both for co- and counter-rotating OAM modes, as a multimode generalization of the result obtained in Ref. [68]. Another curious feature of the nonlinear coupling is the reduction of the apparent multimode to an effective three-mode dynamics when counter-rotating vortices are mixed. The dynamics of the higher radial modes is *slaved* by the fundamental one, making an effective three-mode coupling.

II. DYNAMICAL EQUATIONS FOR THE COUPLING MODES

We will consider type-II second-harmonic generation in collinear configuration with orthogonally polarized incoming beams carrying arbitrary topological charges. Let us start with the expression for the electric-field vector corresponding to a light wave with the fundamental frequency ω , propagating along the z direction:

$$\mathbf{E}_\omega(\mathbf{r}, z; t) = [\mathcal{E}_h(\mathbf{r}, z) \hat{\mathbf{e}}_h e^{ik_h z} + \mathcal{E}_v(\mathbf{r}, z) \hat{\mathbf{e}}_v e^{ik_v z}] e^{-i\omega t}, \quad (1)$$

where $\hat{\mathbf{e}}_h$ ($\hat{\mathbf{e}}_v$), k_h (k_v), and \mathcal{E}_h (\mathcal{E}_v) are, respectively, the polarization unit vector along the horizontal (vertical) direction, the corresponding wave number, and the transverse spatial function. For type-II phase match the second-harmonic field can be written as

$$\mathbf{E}_{2\omega}(\mathbf{r}, z; t) = \mathcal{E}_{2\omega}(\mathbf{r}, z) \hat{\mathbf{e}}_h e^{i(k_{2\omega} z - 2\omega t)}. \quad (2)$$

*Corresponding author: khoury@if.uff.br

The three field components, (ω, h) , (ω, v) , and (2ω) , follow a coupled evolution inside the nonlinear medium with a coupling constant χ that involves the relevant terms of the nonlinear susceptibility tensor. Under phase match ($k_{2\omega} = k_h + k_v$), the equations describing this coupled evolution in the paraxial approximation are

$$\begin{aligned}\nabla_{\perp}^2 \mathcal{E}_h + 2ik_h \frac{\partial \mathcal{E}_h}{\partial z} &= -\frac{\chi \omega^2}{c^2} \mathcal{E}_{2\omega} \mathcal{E}_v^*, \\ \nabla_{\perp}^2 \mathcal{E}_v + 2ik_v \frac{\partial \mathcal{E}_v}{\partial z} &= -\frac{\chi \omega^2}{c^2} \mathcal{E}_{2\omega} \mathcal{E}_h^*, \\ \nabla_{\perp}^2 \mathcal{E}_{2\omega} + 2ik_{2\omega} \frac{\partial \mathcal{E}_{2\omega}}{\partial z} &= -4 \frac{\chi \omega^2}{c^2} \mathcal{E}_h \mathcal{E}_v,\end{aligned}\quad (3)$$

with $\nabla_{\perp} \equiv (\partial/\partial x, \partial/\partial y)$. In order to inspect the OAM exchange in the nonlinear process, we expand the interacting fields in the Laguerre-Gauss basis:

$$\begin{aligned}\mathcal{E}_h(\mathbf{r}, z) &= \sqrt{\frac{\omega}{n_h}} \sum_{p,l} A_{pl}^h u_{pl}^h(\mathbf{r}, z), \\ \mathcal{E}_v(\mathbf{r}, z) &= \sqrt{\frac{\omega}{n_v}} \sum_{p,l} A_{pl}^v u_{pl}^v(\mathbf{r}, z), \\ \mathcal{E}_{2\omega}(\mathbf{r}, z) &= \sqrt{\frac{2\omega}{n_{2\omega}}} \sum_{p,l} B_{pl} u_{pl}^{2\omega}(\mathbf{r}, z),\end{aligned}\quad (4)$$

where $n_{h(v)}$ is the refraction index for the horizontally (vertically) polarized infrared beam and $n_{2\omega}$ is the second-harmonic refraction index. The orthonormal Laguerre-Gaussian mode functions are

$$u_{pl}^j(\mathbf{r}, z) = \sqrt{\frac{2}{\pi}} \frac{\mathcal{N}_{pl}}{w_j(z)} \left(\frac{\sqrt{2}r}{w_j(z)} \right)^{|l|} L_p^{|l|} \left(\frac{2r^2}{w_j^2(z)} \right) \times e^{-\frac{r^2}{w_j^2(z)}} e^{i \left[\frac{k_j r^2}{2R_j(z)} - (2p+|l|+1) \arctan\left(\frac{z}{z_{R_j}}\right) + l\theta \right]}, \quad (5)$$

$$\mathcal{N}_{pl} = \sqrt{\frac{p!}{(p+|l|)!}} \quad (6)$$

($j = h, v, 2\omega$). The beam width and wavefront radius at position z are, respectively, given by

$$w_j(z) = w_j \sqrt{1 + \left(\frac{z}{z_{R_j}} \right)^2}, \quad (7)$$

$$R_j(z) = z \left[1 + \left(\frac{z_{R_j}}{z} \right)^2 \right], \quad (8)$$

where $w_j = \sqrt{2z_{R_j}/k_j}$ is the beam waist and z_{R_j} is the Rayleigh distance. Besides the longitudinal phase-match condition ($k_h + k_v = k_{2\omega}$), efficient frequency conversion also requires transverse phase match, imposing the wave-front overlap $R_h = R_v = R_{2\omega}$ and a common Rayleigh range $z_{R_h} = z_{R_v} = z_{R_{2\omega}} = z_R$.

This transverse mode decomposition allows the description of the field evolution as a set of coupled equations for the mode

amplitudes [53]:

$$\begin{aligned}\frac{dA_{pl}^h}{dz} &= i g \sum_{p'l'} \sum_{p''l''} \Lambda_{p'p''}^{l'l''} B_{p'l'} (A_{p''l''}^v)^*, \\ \frac{dA_{pl}^v}{dz} &= i g \sum_{p'l'} \sum_{p''l''} \Lambda_{p'p''}^{l'l''} B_{p'l'} (A_{p''l''}^h)^*, \\ \frac{dB_{pl}}{dz} &= i g \sum_{p'l'} \sum_{p''l''} (\Lambda_{pp''}^{l'l''})^* A_{p'l'}^h A_{p''l''}^v.\end{aligned}\quad (9)$$

The following convenient parameters are introduced:

$$g = \frac{\chi}{2c} \sqrt{\frac{2\omega^3}{n_h n_v n_{2\omega}}} R_{000}^{000}, \quad (10)$$

$$\Lambda_{pp''}^{l'l''} = \frac{R_{pp''}^{l'l''}}{R_{000}^{000}}, \quad (11)$$

$$R_{pp''}^{l'l''} = \int u_{pl}^{2\omega} (u_{p'l'}^h)^* (u_{p''l''}^v)^* d^2\mathbf{r}. \quad (12)$$

Here $R_{pp''}^{l'l''}$ is the three-mode spatial overlap of Laguerre-Gauss modes with indices pl , $p'l'$, and $p''l''$.

Equations (9) describe the amplitude evolution of each component in the expansion. We will neglect nonlinear losses ($\chi^* = \chi$) and the Gouy phase acquired inside the crystal, making $(\Lambda_{pp''}^{l'l''})^* = \Lambda_{pp''}^{l'l''}$. In fact, from the experimental values of the infrared and second-harmonic beam waists, which were on the order of 0.2–0.4 mm, the Rayleigh range was around tens of centimeters while the crystal was only 10 mm long. In this case, the factor $\arctan(z/z_R)$ can be fairly neglected within the interaction distance. The Gouy phases of the generated modes only show up in the diffraction region where the nonlinear interaction no longer occurs.

A. Effective nonlinear mode coupling

In the multimode dynamics, the effective nonlinear coupling between the different modes is basically ruled by the nonlinear susceptibility χ and the spatial overlap integral defined in Eq. (12). Here we are interested in the nonlinear OAM mixing of two beams carrying topological charges l' and l'' , with zero radial order ($p' = p'' = 0$). In Appendix A, the calculation of the corresponding overlap integral is detailed and two selection rules are derived. The first one leads to the expected OAM conservation, already discussed in previous works [43,44,46,51,52]. The second one is less obvious and predicts that higher radial orders are generated in the second-harmonic field when opposite helicities are combined in the nonlinear process.

When both input topological charges have the same sign ($l' \cdot l'' \geq 0$), the normalized overlap becomes

$$\Lambda_{p00}^{l'l''} = \delta_{l,l'+l''} \begin{cases} \sqrt{\frac{\xi_h^{|l'|} \xi_v^{|l''|} (|l'|+|l''|)!}{|l'|!|l''|!}} & (p=0), \\ 0 & (p>0), \end{cases} \quad (13)$$

where $\xi_j \equiv (w_{2\omega}/w_j)^2$. This means that the two input modes couple to a single second-harmonic one carrying the added

topological charge $l = l' + l''$ (OAM conservation) and having zero radial order ($p = 0$).

A less intuitive situation is produced when the input modes carry topological charges with opposite signs ($l' \cdot l'' < 0$). In this case, the resulting overlap integral becomes

$$\Lambda_{p00}^{l'l''} = \delta_{l,l'+l''} \begin{cases} \frac{(-1)^p}{(P-p)!} \sqrt{\frac{\xi_h^{l'} \xi_v^{l''} |l'|! |l''|!}{p!(p+|l'+l''|)!}} & (p \leq P), \\ 0 & (p > P), \end{cases} \quad (14)$$

where $P = \min(|l'|, |l''|)$, so that higher radial orders, up to the minimum value between $|l'|$ and $|l''|$, are generated in the second-harmonic field. Therefore, the nonlinear mixing of opposite helicities implies a more complex dynamics with more transverse modes taking part in the nonlinear interaction.

B. Multimode Manley-Rowe relations

In order to derive multimode conservation laws, it will be useful to define the phase (ϕ_{pl}^j, ψ_{pl}) and intensity (I_{pl}^j, J_{pl}) variables, in terms of which the mode amplitudes are expressed as

$$A_{pl}^{h(v)} = \sqrt{I_{pl}^{h(v)}} e^{i\phi_{pl}^{h(v)}}, \quad B_{pl} = \sqrt{J_{pl}} e^{i\psi_{pl}}. \quad (15)$$

In Appendix A we derive the following Manley-Rowe relations:

$$\begin{aligned} \sum_{p'l''} I_{p'l''}^v(z) - \sum_{p'l'} I_{p'l'}^h(z) &= \sum_{p'l''} I_{p'l''}^v(0) - \sum_{p'l'} I_{p'l'}^h(0), \\ \sum_{pl} J_{pl}(z) + \sum_{p'l'} I_{p'l'}^{h,v}(z) &= \sum_{pl} J_{pl}(0) + \sum_{p'l'} I_{p'l'}^{h,v}(0). \end{aligned} \quad (16)$$

These conservation laws are important for the solutions of the dynamical equations. They identify the natural integration constants for the dynamical equations.

III. NONLINEAR MIXING OF COROTATING VORTICES

We now solve the nonlinear coupled equations for the three-mode interaction in second-harmonic generation of corotating vortices. As we discussed in Sec. II A, when two corotating vortices with zero radial order are mixed in the nonlinear process, a single second-harmonic mode will be excited and a three-mode dynamics is realized. In this case, Eqs. (9) are significantly simplified and an analytical solution can be found. For this purpose we assume only two nonzero initial amplitudes ($l' = m$ and $l'' = n$) $A_{0m}^h(0) = A_{0n}^v(0) = \sqrt{I_0}$ ($m \cdot n \geq 0$) at the crystal entrance, all other modes being empty. According to the overlap integrals given by Eq. (13), a single second-harmonic mode with $p = 0$ and $l = m + n$ will be excited. The resulting three-mode dynamical equations are

$$\begin{aligned} \frac{dA_{0m}^h}{dz} &= i g \Lambda_{000}^{mn} B_0 A_{0n}^{v*}, \\ \frac{dA_{0n}^v}{dz} &= i g \Lambda_{000}^{mn} B_0 A_{0m}^{h*}, \\ \frac{dB_0}{dz} &= i g \Lambda_{000}^{mn} A_{0m}^h A_{0n}^v, \end{aligned} \quad (17)$$

where B_0 is the second-harmonic amplitude with zero radial order ($p = 0$) and we omitted the superfluous index l for

simplicity. Equations (17) can be further simplified by defining the following rescaled amplitudes:

$$b = g \Lambda_{000}^{mn} B_0, \quad a_h = g \Lambda_{000}^{mn} A_{0m}^h, \quad a_v = g \Lambda_{000}^{mn} A_{0n}^v, \quad (18)$$

giving

$$\frac{da_h}{dz} = i b a_v^*, \quad \frac{da_v}{dz} = i b a_h^*, \quad \frac{db}{dz} = i a_h a_v. \quad (19)$$

The analytical solution for this system is derived in Appendix C. It resembles the original solution found in Ref. [68]. The resulting output intensities are

$$\begin{aligned} J_0(z) &= 2I_0 \tanh^2(g \Lambda_{000}^{mn} \sqrt{2I_0} z), \\ I_{0n}^v(z) = I_{0m}^h(z) &= I_0 \operatorname{sech}^2(g \Lambda_{000}^{mn} \sqrt{2I_0} z), \end{aligned} \quad (20)$$

where $I_{0m}^h = |A_{0m}^h|^2$, $I_{0n}^v = |A_{0n}^v|^2$, $J_0 = |B_0|^2$, and $I_0 = I_{0m}^h(0) = I_{0n}^v(0)$ is the common intensity of the input modes at the crystal entrance. Moreover, along the interaction distance z the phase variables evolve under the following phase-match condition:

$$\phi_{0m}^h(z) + \phi_{0n}^v(z) - \psi_0(z) = (2N + 1) \frac{\pi}{2}, \quad (21)$$

with $N \in \mathbb{Z}$, as detailed in Appendix C.

IV. HIGHER RADIAL ORDERS GENERATION FROM COUNTER-ROTATING VORTICES

We now investigate the generation of arbitrary radial orders from the orbital-angular-momentum mixing of counter-rotating vortices. As we have already mentioned, radial orders up to the minimum absolute value of the mixed OAM are generated in the process. In principle, this could imply a complicated multimode dynamics, but we demonstrate that an effective three-mode dynamics can be derived. Let us consider the input modes A_{0m}^h and A_{0n}^v , with $m \cdot n < 0$. Without loss of generality, we shall assume $|m| < |n|$. In this case, the dynamical equations are

$$\frac{dA_{0m}^h}{dz} = i g A_{0n}^{v*} \sum_{p=0}^{|m|} \Lambda_{p00}^{mn} B_p, \quad (22)$$

$$\frac{dA_{0n}^v}{dz} = i g A_{0m}^{h*} \sum_{p=0}^{|m|} \Lambda_{p00}^{mn} B_p, \quad (23)$$

$$\frac{dB_p}{dz} = i g \Lambda_{p00}^{mn} A_{0m}^h A_{0n}^v \quad (0 \leq p \leq |m|), \quad (24)$$

where B_p is the amplitude of the second-harmonic radial mode p . Note that Eq. (24) imposes the relation

$$\frac{dB_p}{dz} = \frac{\Lambda_{p00}^{mn}}{\Lambda_{000}^{mn}} \frac{dB_0}{dz}. \quad (25)$$

This relation implies a constrained evolution of the second-harmonic mode amplitudes. Assuming null second-harmonic input [$B_p(0) = 0$], we obtain

$$B_p(z) = \frac{\Lambda_{p00}^{mn}}{\Lambda_{000}^{mn}} B_0(z). \quad (26)$$

By defining the rescaled amplitudes

$$b = g \frac{\Lambda_{\text{eff}}^2}{\Lambda_{000}^2} B_0, \quad (27)$$

$$a_h = g \Lambda_{\text{eff}} A_{0m}^h, \quad (28)$$

$$a_v = g \Lambda_{\text{eff}} A_{0n}^v, \quad (29)$$

$$\Lambda_{\text{eff}} \equiv \left[\sum_{p=0}^{|m|} (\Lambda_{p00}^{mn})^2 \right]^{1/2}, \quad (30)$$

we arrive at an effective three-mode coupling, governed by the same rescaled dynamical equations (19). Therefore, the orbital-angular-momentum mixing of counter-rotating vortices gives rise to a superposition of radial modes, locked in phase and amplitude as determined by Eq. (26). In some sense, this phase and amplitude locking among the radial modes can be considered analogous to the longitudinal mode locking achieved in pulsed laser cavities.

For the initial condition $A_{0m}^h(0) = A_{0n}^v(0) = \sqrt{I_0}$, the analytical solutions for the output intensities are derived in Appendix C:

$$\begin{aligned} I_{0n}^v(z) &= I_{0m}^h(z) = I_0 \operatorname{sech}^2(g \Lambda_{\text{eff}} \sqrt{2I_0} z), \\ J_0(z) &= 2I_0 \left(\frac{\Lambda_{000}^{mn}}{\Lambda_{\text{eff}}} \right)^2 \tanh^2(g \Lambda_{\text{eff}} \sqrt{2I_0} z), \\ J_p(z) &= \left(\frac{\Lambda_{p00}^{mn}}{\Lambda_{000}^{mn}} \right)^2 J_0(z). \end{aligned} \quad (31)$$

Therefore, the second-harmonic field generated by counter-rotating vortices is a superposition of transverse modes carrying the same topological charge, but with different radial orders. Since the LG mode order is $2p + |l|$, the different modes in the second-harmonic field acquire different Gouy phases along propagation, making different near- and far-field images. This will be used in our experimental investigation to evidence the multimode structure of the second-harmonic field.

V. EXPERIMENTAL RESULTS

Our experimental setup is sketched in Fig. 1. Two beams from an infrared Nd:YAG laser (wavelength $\lambda = 1064$ nm) impinge on two half screens of a spatial light modulator. Each

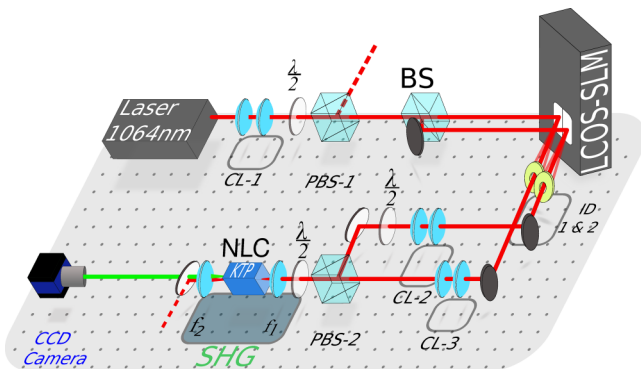


FIG. 1. Experimental setup.

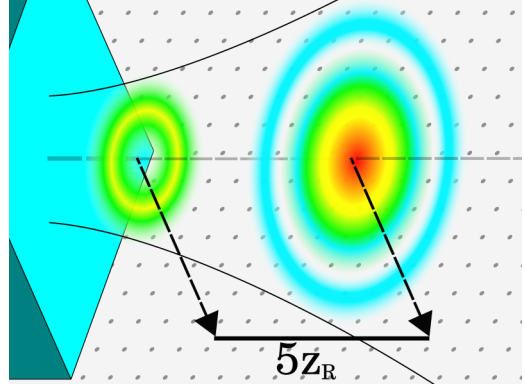


FIG. 2. Sketch of the multiradial mode propagation, showing the transition between the near- and far-field images.

half screen is computer controlled to generate an independent OAM hologram and produce arbitrary pairs of topological charges. The two OAM beams produced are then set with orthogonal polarizations and pass through pairs of collimating lenses for mode matching before being superposed on a polarizing beam splitter (PBS). After the PBS, the orthogonally polarized OAM beams are focused on a potassium titanyl phosphate crystal cut for type-II phase match. The second-harmonic beam at 532-nm wavelength is separated from the fundamental beam by a spectral filter and sent to an imaging system.

The waists of the infrared and second-harmonic beams were on the order of 0.2–0.4 mm, which corresponds to a Rayleigh distance of tens of centimeters. Since the crystal was only 10 mm long, the factor $\arctan(z/z_R)$ can be fairly neglected within the interaction distance and the Gouy phases only show up in the diffraction region where the nonlinear interaction no longer occurs. In order to evidence the generation of higher radial orders experimentally, we performed intensity measurements on the second-harmonic beam both in the near- and far-field regions. The superposition of different radial orders carrying the same topological charge involves modes acquiring different Gouy phases $(2p + |l| + 1) \arctan(z/z_R)$ along propagation. This results in different near- and far-field images of the second harmonic, as suggested by the propagation sketch shown in Fig. 2. The image evolution can be easily simulated and compared to the experimental images acquired with a CCD camera placed in different propagation regions. The corresponding images are displayed in Fig. 3. While the near-field images only display a hollow intensity distribution, the appearance of external rings in the far-field intensity patterns unravels the presence of higher radial orders. Moreover, the phase singularity remains present in the far field when there is a net OAM transferred to the second harmonic. In these cases, the phase singularity and the external rings coexist in the far-field intensity distribution. The agreement between the experimental results and the simulated images is remarkable.

An intuitive picture can be envisaged for the far-field structure of the second harmonic produced by opposite topological charges ($l' = -l''$). In this case, the second harmonic carries no OAM, but has a hollow intensity distribution in the near field. Therefore, the far-field structure is analogous to the diffraction

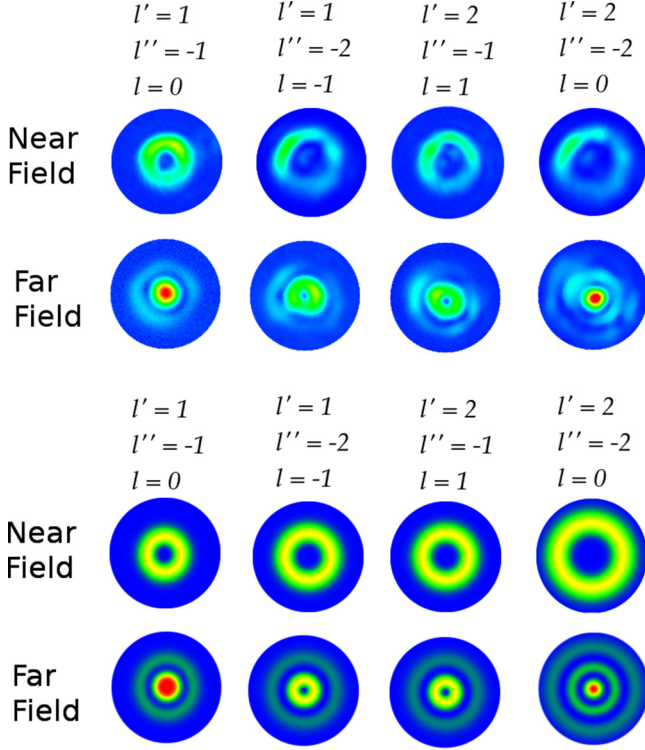


FIG. 3. Experimental (top) and theoretical simulation (bottom) of the near- and far-field images formed by second-harmonic generation of counter-rotating vortices.

pattern produced by a circular obstacle and the central peak can be viewed as a manifestation of the famous Poisson spot, which by the way also comes accompanied by external rings. Of course, in the usual Poisson spot situation, a sharp circular obstacle is assumed, giving rise to a virtually infinite number of external rings. However, the near-field pattern of the second harmonic generated by opposite input charges has a smooth hollow distribution. Therefore, the far-field pattern will exhibit a limited number of external rings, precisely equal to the absolute value of the mutually annihilating charges. This suggests a further method for topological charge measurement through the nonlinear mixing of a sample OAM beam with its mirror image.

VI. CONCLUSION

We developed a detailed study of the orbital-angular-momentum mixing in type-II second-harmonic generation. The multimode nonlinear dynamical equations were derived and solved. Special attention was given to the selection rules determining the transverse mode coupling in the nonlinear medium. While the well-known OAM conservation condition is recovered, a less trivial condition was derived for the radial modes. The generation of higher radial orders, when counter-rotating vortices are mixed, is a subtle effect predicted by our theoretical approach and confirmed by our experimental results. For opposite input charges, it allows an interesting interpretation in terms of the famous Poisson spot and can be viewed as a further method for OAM measurement.

Another interesting feature is the effective three-mode dynamics obtained even when higher radial orders are generated. These higher radial orders are phase and amplitude locked to the fundamental radial mode, producing a kind of transverse mode locking.

ACKNOWLEDGMENTS

The authors acknowledge financial support from the Brazilian funding agencies Fundação Carlos Chagas Filho de Amparo à Pesquisa do Estado do Rio de Janeiro (FAPERJ), Coordenação de Aperfeiçoamento de Pessoal de Nível Superior (CAPES), Conselho Nacional de Desenvolvimento Científico e Tecnológico (CNPq) and Instituto Nacional de Ciência e Tecnologia de Informação Quântica (INCT-IQ-CNPq).

APPENDIX A: SPATIAL OVERLAP AND SELECTION RULES

We now calculate explicitly the overlap integrals giving rise to OAM conservation and radial order selection rules. The effective nonlinear coupling between modes $(p, l; 2\omega)$, $(p', l'; \omega, h)$, and $(p'', l''; \omega, v)$ is determined by the following overlap integral:

$$R_{pp'p''}^{ll'l''} = \sqrt{\frac{8}{\pi^3}} \frac{\mathcal{N}_{pl}\mathcal{N}_{p'l'}\mathcal{N}_{p''l''}}{w_h w_v w_{2\omega}} \int_0^\infty r dr \frac{(\sqrt{2}r)^{|l|+|l'|+|l''|}}{w_{2\omega}^{|l|} w_h^{|l'|} w_v^{|l''|}} \times L_p^{|l|} \left(\frac{2r^2}{w_{2\omega}^2} \right) L_{p'}^{|l'|} \left(\frac{2r^2}{w_h^2} \right) L_{p''}^{|l''|} \left(\frac{2r^2}{w_v^2} \right) \times e^{-\left(\frac{r^2}{w_{2\omega}^2} + \frac{r^2}{w_h^2} + \frac{r^2}{w_v^2}\right)} \int_0^{2\pi} d\theta e^{i(l-l'-l'')\theta}. \quad (\text{A1})$$

Note that the phase-match ($k_h + k_v = k_{2\omega}$) and wave-front match ($z_{R_h} = z_{R_v} = z_{R_{2\omega}}$) conditions allow the cancellation of the curved wave-front contributions and imply the following relationship between the mode widths:

$$\frac{1}{w_{2\omega}^2} = \frac{1}{w_h^2} + \frac{1}{w_v^2}. \quad (\text{A2})$$

Moreover, the angular integral provides the OAM selection rule $l = l' + l''$, so that the overlap integral can be written as

$$R_{pp'p''}^{ll'l''} = \sqrt{\frac{2}{\pi}} \delta_{l, l'+l''} \frac{\mathcal{N}_{pl}\mathcal{N}_{p'l'}\mathcal{N}_{p''l''}}{w_{2\omega}} \sqrt{\xi_h^{|l'+1|} \xi_v^{|l''+1|}} \times \int_0^\infty x^{\frac{|l|+|l'|+|l''|}{2}} L_p^{|l|}(x) L_{p'}^{|l'|}(\xi_h x) L_{p''}^{|l''|}(\xi_v x) e^{-x} dx, \quad (\text{A3})$$

where we defined

$$x = \frac{2r^2}{w_{2\omega}^2}, \quad \xi_j = \left(\frac{w_{2\omega}}{w_j} \right)^2. \quad (\text{A4})$$

The fundamental modes overlap is

$$R_{000}^{000} = \sqrt{\frac{2}{\pi}} \frac{\sqrt{\xi_h \xi_v}}{w_{2\omega}}. \quad (\text{A5})$$

The overlap integral normalized to the fundamental modes overlap becomes

$$\begin{aligned} \Lambda_{pp'p''}^{l'l''} &= \delta_{l,l'+l''} \mathcal{N}_{pl} \mathcal{N}_{p'l'} \mathcal{N}_{p''l''} \sqrt{\xi_h^{l'} \xi_v^{l''}} \\ &\times \int_0^\infty x^{\frac{|l'+l''|}{2}} L_p^{l'}(x) L_{p'}^{l'}(\xi_h x) L_{p''}^{l''}(\xi_v x) e^{-x} dx. \end{aligned} \quad (\text{A6})$$

We will be interested in the generation of higher radial orders from zeroth-order input beams, so we assume that the incoming modes have no radial structure and restrict our analysis to $p' = p'' = 0$. By using $L_0^k(x) = 1$ and making $P = \min(|l'|, |l''|) = (|l'| + |l''| - |l' + l''|)/2$, the spatial overlap integral assumes the following simplified form:

$$\begin{aligned} \Lambda_{p00}^{l'l''} &= \sqrt{\frac{\xi_h^{l'} \xi_v^{l''} p!}{(p + |l' + l''|)! |l'|! |l''|!}} \\ &\times \int_0^\infty x^{|l'+l''|} x^P L_p^{l'+l''}(x) e^{-x} dx, \end{aligned} \quad (\text{A7})$$

where we have omitted the superfluous index l . From the recurrence relations for the generalized Laguerre polynomials, one readily derives a useful expansion for the monomial:

$$x^P = \sum_{m=0}^P \frac{(-1)^m P! (k+P)!}{(P-m)! (k+m)!} L_m^k(x), \quad (\text{A8})$$

which can be used together with the orthogonality relations,

$$\int_0^\infty x^k L_n^k(x) L_m^k(x) e^{-x} dx = \frac{(n+k)!}{n!} \delta_{nm}, \quad (\text{A9})$$

to derive the final result

$$\Lambda_{p00}^{l'l''} = \begin{cases} \frac{(-1)^p \sqrt{\xi_h^{l'} \xi_v^{l''}} P! (P+|l'+l''|)!}{(P-p)! \sqrt{p! (p+|l'+l''|)! |l'|! |l''|!}} & (p \leq P), \\ 0 & (p > P). \end{cases} \quad (\text{A10})$$

Now, two different situations need to be treated separately, depending on the relative helicities of the incoming modes. They lead to the radial selection rules for the second-harmonic field.

(1) Corotating vortices: $l' \cdot l'' \geq 0$. This corresponds to $P = 0$, giving

$$\Lambda_{p00}^{l'l''} = \begin{cases} \sqrt{\frac{\xi_h^{l'} \xi_v^{l''} (|l'|+|l''|)!}{|l'|! |l''|!}} & (p = 0), \\ 0 & (p > 0). \end{cases} \quad (\text{A11})$$

No higher radial orders are generated in the second-harmonic field in this case.

(2) Counter-rotating vortices: $l' \cdot l'' < 0$. This corresponds to $P = \min(|l'|, |l''|)$, giving

$$\Lambda_{p00}^{l'l''} = \begin{cases} \frac{(-1)^p \sqrt{\xi_h^{l'} \xi_v^{l''}} |l'|! |l''|!}{(P-p)! \sqrt{p! (p+|l'+l''|)!}} & (p \leq P), \\ 0 & (p > P). \end{cases} \quad (\text{A12})$$

Higher radial orders are generated in the second-harmonic field up to the minimum value between $|l'|$ and $|l''|$.

APPENDIX B: MULTIMODE MANLEY-ROWE RELATIONS

In order to derive a set of multimode Manley-Rowe relations, the mode amplitudes are decomposed in terms of phase and intensity variables as

$$A_{pl}^i = \sqrt{I_{pl}^i} e^{i\phi_{pl}^i}, \quad B_{pl} = \sqrt{J_{pl}} e^{i\psi_{pl}}. \quad (\text{B1})$$

In terms of these variables, the dynamical equations become

$$\begin{aligned} &\left(\frac{d\sqrt{I_{p'l'}^h}}{dz} + i\sqrt{I_{p'l'}^h} \frac{d\phi_{p'l'}^h}{dz} \right) e^{i\phi_{p'l'}^h} \\ &= ig \sum_{pl} \sum_{p''l''} \Lambda_{pp'p''}^{l'l''} \sqrt{J_{pl} I_{p'l''}^v} e^{i(\psi_{pl} - \phi_{p''l''}^v)}, \end{aligned} \quad (\text{B2})$$

$$\begin{aligned} &\left(\frac{d\sqrt{I_{p'l''}^v}}{dz} + i\sqrt{I_{p'l''}^v} \frac{d\phi_{p'l''}^v}{dz} \right) e^{i\phi_{p'l''}^v} \\ &= ig \sum_{pl} \sum_{p'l'} \Lambda_{pp'p''}^{l'l''} \sqrt{J_{pl} I_{p'l'}^h} e^{i(\psi_{pl} - \phi_{p'l'}^h)}, \end{aligned} \quad (\text{B3})$$

$$\begin{aligned} &\left(\frac{d\sqrt{J_{pl}}}{dz} + i\sqrt{J_{pl}} \frac{d\psi_{pl}}{dz} \right) e^{i\psi_{pl}} \\ &= ig \sum_{p'l'} \sum_{p''l''} \Lambda_{pp'p''}^{l'l''} \sqrt{I_{p'l'}^h I_{p'l''}^v} e^{i(\phi_{p'l'}^h + \phi_{p'l''}^v)}. \end{aligned} \quad (\text{B4})$$

Taking the real and imaginary parts, we arrive at the phase-intensity dynamical equations:

$$\begin{aligned} \frac{dI_{p'l'}^h}{dz} &= 2g \sum_{pl, p''l''} \Lambda_{pp'p''}^{l'l''} \sqrt{J_{pl} I_{p'l'}^h I_{p'l''}^v} \sin \Delta_{pp'p''}^{l'l''}, \\ \frac{dI_{p'l''}^v}{dz} &= 2g \sum_{pl, p'l'} \Lambda_{pp'p''}^{l'l''} \sqrt{J_{pl} I_{p'l'}^h I_{p'l''}^v} \sin \Delta_{pp'p''}^{l'l''}, \end{aligned} \quad (\text{B5})$$

$$\begin{aligned} \frac{dJ_{pl}}{dz} &= -2g \sum_{p'l', p''l''} \Lambda_{pp'p''}^{l'l''} \sqrt{J_{pl} I_{p'l'}^h I_{p'l''}^v} \sin \Delta_{pp'p''}^{l'l''}, \\ I_{p'l'}^h \frac{d\phi_{p'l'}^h}{dz} &= g \sum_{pl, p''l''} \Lambda_{pp'p''}^{l'l''} \sqrt{J_{pl} I_{p'l'}^h I_{p'l''}^v} \cos \Delta_{pp'p''}^{l'l''}, \end{aligned}$$

$$I_{p'l''}^v \frac{d\phi_{p'l''}^v}{dz} = g \sum_{pl, p'l'} \Lambda_{pp'p''}^{l'l''} \sqrt{J_{pl} I_{p'l'}^h I_{p'l''}^v} \cos \Delta_{pp'p''}^{l'l''}, \quad (\text{B6})$$

$$J_{pl} \frac{d\psi_{pl}}{dz} = g \sum_{p'l', p''l''} \Lambda_{pp'p''}^{l'l''} \sqrt{J_{pl} I_{p'l'}^h I_{p'l''}^v} \cos \Delta_{pp'p''}^{l'l''},$$

where $\Delta_{pp'p''}^{l'l''} = \phi_{p'l'}^h + \phi_{p'l''}^v - \psi_{pl}$. From these equations of motion, we derive the conservation laws given by generalized Manley-Rowe relations. The first relation is derived by adding up the intensity equations of motion for all Laguerre-Gaussian components of the down converted fields, giving

$$\frac{d}{dz} \sum_{pl} (I_{p'l}^v - I_{pl}^h) = 0, \quad (\text{B7})$$

which simply states that the total intensity difference between signal and idler fields remains constant along the nonlinear process.

The second relation is derived by adding up the intensity equations of motion for the Laguerre-Gaussian components of the second-harmonic field and comparing with the previous result obtained for the down converted fields, which gives the following relation:

$$\frac{d}{dz} \sum_{pl} (J_{pl} + I_{pl}^h) = \frac{d}{dz} \sum_{pl} (J_{pl} + I_{pl}^v) = 0. \quad (\text{B8})$$

These conservation laws help identifying the natural integration constants of the nonlinear dynamical equations. They will be used in the derivation of their analytical solutions.

APPENDIX C: THREE-MODE ANALYTICAL SOLUTION

We derive the analytical solution for the three-mode evolution in second-harmonic generation as described by the rescaled nonlinear equations:

$$\frac{da_h}{dz} = i b a_v^*, \quad \frac{da_v}{dz} = i b a_h^*, \quad \frac{db}{dz} = i a_h a_v. \quad (\text{C1})$$

Let us define the phase-intensity variables according to

$$a_h = \sqrt{\bar{I}_h} e^{i\phi_h}, \quad a_v = \sqrt{\bar{I}_v} e^{i\phi_v}, \quad b = \sqrt{\bar{J}} e^{i\psi}. \quad (\text{C2})$$

The phase-intensity dynamical equations are of the general form

$$\begin{aligned} \frac{d\bar{I}_h}{dz} &= 2\sqrt{\bar{J}\bar{I}_h\bar{I}_v} \sin(\phi_h + \phi_v - \psi), \\ \frac{d\bar{I}_v}{dz} &= 2\sqrt{\bar{J}\bar{I}_h\bar{I}_v} \sin(\phi_h + \phi_v - \psi), \\ \frac{d\bar{J}}{dz} &= -2\sqrt{\bar{J}\bar{I}_h\bar{I}_v} \sin(\phi_h + \phi_v - \psi), \\ \bar{I}_h \frac{d\phi_h}{dz} &= \sqrt{\bar{J}\bar{I}_h\bar{I}_v} \cos(\phi_h + \phi_v - \psi), \end{aligned}$$

$$\begin{aligned} \bar{I}_v \frac{d\phi_v}{dz} &= \sqrt{\bar{J}\bar{I}_h\bar{I}_v} \cos(\phi_h + \phi_v - \psi), \\ \bar{J} \frac{d\psi}{dz} &= \sqrt{\bar{J}\bar{I}_h\bar{I}_v} \cos(\phi_h + \phi_v - \psi). \end{aligned} \quad (\text{C3})$$

From these phase-intensity equations it can be straightforwardly demonstrated that

$$\frac{d}{dz} \left(\bar{J} \frac{d\psi}{dz} \right) = \frac{d}{dz} \left(\bar{I}_h \frac{d\phi_h}{dz} \right) = \frac{d}{dz} \left(\bar{I}_v \frac{d\phi_v}{dz} \right) = 0, \quad (\text{C4})$$

giving the following conserved quantity:

$$\sqrt{\bar{I}_h(z)\bar{I}_v(z)\bar{J}(z)} \cos \Phi(z) = \sqrt{\bar{I}_h(0)\bar{I}_v(0)\bar{J}(0)} \cos \Phi(0), \quad (\text{C5})$$

where $\Phi(z) \equiv \phi_h(z) + \phi_v(z) - \psi(z)$. If the second-harmonic field is not seeded, then $\bar{J}(0) = 0$ and this conserved quantity imposes $\cos \Phi(z) = 0$ for nonvanishing solutions for $\bar{J}(z)$. In this case, one immediately sees from the phase equations that ϕ_h , ϕ_v , and ψ are stationary and must fulfill $\Phi(z) = (2n + 1)\pi/2$.

In order to derive the analytical solution for the three-mode evolution, we assume that the input fields have equal intensities $\bar{I}_v(0) = \bar{I}_h(0) = \bar{I}_0$. From the Manley-Rowe relations one has

$$\bar{I}_v(z) = \bar{I}_h(z), \quad (\text{C6})$$

$$\bar{J}(z) = 2[\bar{I}_0 - \bar{I}_h(z)], \quad (\text{C7})$$

so that the dynamical equation for \bar{I}_h assumes the simple form

$$\frac{d\bar{I}_h}{dz} = 2\sqrt{2(\bar{I}_0 - \bar{I}_h)} \bar{I}_h, \quad (\text{C8})$$

which can be readily solved, giving the well-known hyperbolic solutions for the interacting field intensities:

$$\begin{aligned} \bar{I}_h(z) = \bar{I}_v(z) &= \bar{I}_0 \operatorname{sech}^2(\sqrt{2\bar{I}_0} z), \\ \bar{J}(z) &= 2\bar{I}_0 \tanh^2(\sqrt{2\bar{I}_0} z). \end{aligned} \quad (\text{C9})$$

-
- [1] M. Padgett, *Opt. Express* **25**, 11265 (2017).
 [2] M. J. Padgett and J. Courtial, *Opt. Lett.* **24**, 430 (1999).
 [3] M. França Santos, P. Milman, A. Z. Khoury, and P. H. Souto Ribeiro, *Phys. Rev. A* **64**, 023804 (2001).
 [4] D. P. Caetano, P. H. Souto Ribeiro, J. T. C. Pardal, and A. Z. Khoury, *Phys. Rev. A* **68**, 023805 (2003).
 [5] C. E. R. Souza, J. A. O. Huguenin, P. Milman, and A. Z. Khoury, *Phys. Rev. Lett.* **99**, 160401 (2007).
 [6] E. Nagali, F. Sciarrino, F. De Martini, L. Marrucci, B. Piccirillo, E. Karimi, and E. Santamato, *Phys. Rev. Lett.* **103**, 013601 (2009).
 [7] B. N. Simon, S. Simon, F. Gori, M. Santarsiero, R. Borghi, N. Mukunda, and R. Simon, *Phys. Rev. Lett.* **104**, 023901 (2010).
 [8] A. Holleczek, A. Aiello, C. Gabriel, C. Marquardt, and G. Leuchs, *Opt. Express* **19**, 9714 (2011).
 [9] F. Cardano, E. Karimi, S. Slussarenko, L. Marrucci, C. de Lisio, and E. Santamato, *Appl. Opt.* **51**, C1 (2012).
 [10] G. Milione, A. Dudley, T. A. Nguyen, K. Chakraborty, E. Karimi, A. Forbes, and R. R. Alfano, *J. Opt.* **17**, 035617 (2015).
 [11] A. Aiello, F. Töppel, C. Marquardt, E. Giacobino, and G. Leuchs, *New J. Phys.* **17**, 043024 (2015).
 [12] J. Harris, V. Grillo, E. Mafakheri, G. C. Gazzadi, S. Frabboni, R. W. Boyd, and E. Karimi, *Nat. Phys.* **11**, 629 (2015).
 [13] G. Milione, T. A. Nguyen, J. Leach, D. A. Nolan, and R. R. Alfano, *Opt. Lett.* **40**, 4887 (2015).

- [14] Z.-Y. Zhou, Y. Li, D.-S. Ding, W. Zhang, S. Shi, and B.-S. Shi, *Opt. Express* **23**, 18435 (2015).
- [15] L. Chen and W. She, *Phys. Rev. A* **80**, 063831 (2009).
- [16] J. T. Barreiro, T.-C. Wei, and P. G. Kwiat, *Phys. Rev. Lett.* **105**, 030407 (2010).
- [17] A. Z. Khoury and P. Milman, *Phys. Rev. A* **83**, 060301(R) (2011).
- [18] S. M. Hashemi Rafsanjani, M. Mirhosseini, O. S. Magaña-Loaiza, and R. W. Boyd, *Phys. Rev. A* **92**, 023827 (2015).
- [19] M. Erhard, H. Qassim, H. Mand, E. Karimi, and R. W. Boyd, *Phys. Rev. A* **92**, 022321 (2015).
- [20] D. Guzman-Silva, R. Brüning, F. Zimmermann, C. Vetter, M. Gräfe, M. Heinrich, S. Nolte, M. Duparré, A. Aiello, M. Ornigotti, and A. Szameit, *Laser Photon. Rev.* **10**, 317 (2016).
- [21] B. Pinheiro da Silva, M. Astigarreta Leal, C. E. R. Souza, E. F. Galvão, and A. Z. Khoury, *J. Phys. B* **49**, 055501 (2016).
- [22] L. Aolita and S. P. Walborn, *Phys. Rev. Lett.* **98**, 100501 (2007).
- [23] C. E. R. Souza, C. V. S. Borges, A. Z. Khoury, J. A. O. Huguenin, L. Aolita, and S. P. Walborn, *Phys. Rev. A* **77**, 032345 (2008).
- [24] V. D'Ambrosio, E. Nagali, S. P. Walborn, L. Aolita, S. Slussarenko, L. Marrucci, and F. Sciarrino, *Nat. Commun.* **3**, 961 (2012).
- [25] A. N. de Oliveira, S. P. Walborn, and C. H. Monken, *J. Opt. B* **7**, 288 (2005).
- [26] C. E. R. Souza and A. Z. Khoury, *Opt. Express* **18**, 9207 (2010).
- [27] A. R. C. Pinheiro, C. E. R. Souza, D. P. Caetano, J. A. O. Huguenin, A. G. M. Schmidt, and A. Z. Khoury, *J. Opt. Soc. Am. B* **30**, 3210 (2013).
- [28] M. Hor-Meyll, A. Auyuanet, C. V. S. Borges, A. Aragão, J. A. O. Huguenin, A. Z. Khoury, and L. Davidovich, *Phys. Rev. A* **80**, 042327 (2009).
- [29] F. Töppel, A. Aiello, C. Marquardt, E. Giacobino, and G. Leuchs, *New J. Phys.* **16**, 073019 (2014).
- [30] M. McLaren, T. Konrad, and A. Forbes, *Phys. Rev. A* **92**, 023833 (2015).
- [31] B. Ndagano, B. Perez-Garcia, F. S. Roux, M. McLaren, C. Rosales-Guzman, Y. Zhang, O. Mouane, R. I. Hernandez-Aranda, T. Konrad, and A. Forbes, *Nat. Phys.* **13**, 397 (2017).
- [32] C. V. S. Borges, M. Hor-Meyll, J. A. O. Huguenin, and A. Z. Khoury, *Phys. Rev. A* **82**, 033833 (2010).
- [33] L. Chen and W. She, *J. Opt. Soc. Am. B* **27**, A7 (2010).
- [34] E. Karimi, J. Leach, S. Slussarenko, B. Piccirillo, L. Marrucci, L. X. Chen, W. L. She, S. Franke-Arnold, M. J. Padgett, and E. Santamato, *Phys. Rev. A* **82**, 022115 (2010).
- [35] K. H. Kagalwala, G. Di Giuseppe, A. F. Abouraddy, and B. E. A. Saleh, *Nat. Photon.* **7**, 72 (2013).
- [36] X. F. Qian and J. H. Eberly, *Opt. Lett.* **36**, 4110 (2011).
- [37] L. J. Pereira, A. Z. Khoury, and K. Dechoum, *Phys. Rev. A* **90**, 053842 (2014).
- [38] X. F. Qian, B. Little, J. C. Howell, and J. H. Eberly, *Optica* **2**, 611 (2015).
- [39] W. F. Balthazar, C. E. R. Souza, D. P. Caetano, E. F. Galvão, J. A. O. Huguenin, and A. Z. Khoury, *Opt. Lett.* **41**, 5797 (2016).
- [40] A. Bramati, J.-P. Hermier, A. Z. Khoury, E. Giacobino, P. Schnitzer, R. Michalzik, K. J. Ebeling, J.-Ph. Poizat, and Ph. Grangier, *Opt. Lett.* **24**, 893 (1999).
- [41] J. Courtial, K. Dholakia, L. Allen, and M. J. Padgett, *Phys. Rev. A* **56**, 4193 (1997).
- [42] A. Berzanskis, A. Matijosius, A. Piskarskas, V. Smilgevicus, and A. Stabinis, *Opt. Commun.* **150**, 372 (1998).
- [43] S.-M. Li, L.-J. Kong, Z.-C. Ren, Y. Li, C. Tu, and H.-T. Wang, *Phys. Rev. A* **88**, 035801 (2013).
- [44] W. T. Buono, L. F. C. Moraes, J. A. O. Huguenin, C. E. R. Souza, and A. Z. Khoury, *New J. Phys.* **16**, 093041 (2014).
- [45] Y. Li, Z.-Y. Zhou, D.-S. Ding, and B.-S. Shi, *J. Opt. Soc. Am. B* **32**, 407 (2015).
- [46] A. A. Zhdanova, M. Shutova, A. Bahari, M. Zhi, and A. V. Sokolov, *Opt. Express* **23**, 34109 (2015).
- [47] Y. Li, Z.-Y. Zhou, D.-S. Ding, and B.-S. Shi, *J. Mod. Opt.* **63**, 2271 (2016).
- [48] T. Yusufu, Y. Sasaki, S. Araki, K. Miyamoto, and T. Omatsu, *Appl. Opt.* **55**, 5263 (2016).
- [49] X. Y. Z. Xiong, A. Al-Jarro, L. J. Jiang, N. C. Panoiu, and W. E. I. Sha, *Phys. Rev. B* **95**, 165432 (2017).
- [50] J. Arlt, K. Dholakia, L. Allen, and M. J. Padgett, *Phys. Rev. A* **59**, 3950 (1999).
- [51] A. Mair, A. Vaziri, G. Weihs, and A. Zeilinger, *Nature (London)* **412**, 313 (2001).
- [52] D. P. Caetano, M. P. Almeida, P. H. Souto Ribeiro, J. A. O. Huguenin, B. Coutinho dos Santos, and A. Z. Khoury, *Phys. Rev. A* **66**, 041801 (2002).
- [53] C. Schwob, P. F. Cohadon, C. Fabre, M. A. M. Marte, H. Ritsch, A. Gatti, and L. Lugiato, *Appl. Phys. B* **66**, 685 (1998).
- [54] M. Martinelli, J. A. O. Huguenin, P. Nussenzveig, and A. Z. Khoury, *Phys. Rev. A* **70**, 013812 (2004).
- [55] B. Coutinho dos Santos, A. Z. Khoury, and J. A. O. Huguenin, *Opt. Lett.* **33**, 2803 (2008).
- [56] A. Aadhi, G. K. Samanta, S. C. Kumar, and M. Ebrahim-Zadeh, *Optica* **4**, 349 (2017).
- [57] J. W. R. Tabosa and D. V. Petrov, *Phys. Rev. Lett.* **83**, 4967 (1999).
- [58] S. Barreiro and J. W. R. Tabosa, *Phys. Rev. Lett.* **90**, 133001 (2003).
- [59] G. Walker, A. S. Arnold, and S. Franke-Arnold, *Phys. Rev. Lett.* **108**, 243601 (2012).
- [60] R. Géneaux, A. Camper, T. Auguste, O. Gobert, J. Caillat, R. Taïeb, and T. Ruchon, *Nat. Commun.* **7**, 12583 (2016).
- [61] F. Kong, C. Zhang, F. Bouchard, Z. Li, G. G. Brown, D. H. Ko, T. J. Hammond, L. Arissian, R. W. Boyd, E. Karimi, and P. B. Corkum, *Nat. Commun.* **8**, 14970 (2017).
- [62] R. N. Lanning, Z. Xiao, M. Zhang, I. Novikova, E. E. Mikhailov, and J. P. Dowling, *Phys. Rev. A* **96**, 013830 (2017).
- [63] F. Bouchard, H. Larocque, A. M. Yao, C. Travis, I. De Leon, A. Rubano, E. Karimi, G.-L. Oppo, and R. W. Boyd, *Phys. Rev. Lett.* **117**, 233903 (2016).
- [64] E. Brasselet, *Phys. Rev. A* **82**, 063836 (2010).
- [65] V. N. Belyi, N. A. Khilo, N. S. Kazak, A. A. Ryzhevich, and A. Forbes, *Opt. Eng.* **50**, 059001 (2011).
- [66] Y. Zhang, F. S. Roux, M. McLaren, and A. Forbes, *Phys. Rev. A* **89**, 043820 (2014).
- [67] N. A. Chaitanya, M. V. Jabir, J. Banerji, and G. K. Samanta, *Sci. Rep.* **6**, 32464 (2016).
- [68] J. A. Armstrong, N. Bloembergen, J. Ducuing, and P. S. Pershan, *Phys. Rev.* **127**, 1918 (1962).